


Article

Anomalous Increase in Specific Heat of Binary Molten Salt-Based Graphite Nanofluids for Thermal Energy Storage

Hyun Jung Kim and Byeongnam Jo * 

Department of Mechanical Engineering, Ajou University, Suwon 16499, Korea; hyunkim@ajou.ac.kr

* Correspondence: jo798@ajou.ac.kr; Tel.: +82-31-219-2684

Received: 30 June 2018; Accepted: 3 August 2018; Published: 5 August 2018



Abstract: An anomalous increase of the specific heat was experimentally observed in molten salt nanofluids using a differential scanning calorimeter. Binary carbonate molten salt mixtures were used as a base fluid, and the base salts were doped with graphite nanoparticles. Specific heat measurements of the nanofluids were performed to examine the effects of the composition of two salts consisting of the base fluid. In addition, the effect of the nanoparticle concentration was investigated as the concentration of the graphite nanoparticles was varied from 0.025 to 1.0 wt %. Moreover, the dispersion homogeneity of the nanoparticles was explored by increasing amount of surfactant in the synthesis process of the molten salt nanofluids. The results showed that the specific heat of the nanofluid was enhanced by more than 30% in the liquid phase and by more than 36% in the solid phase at a nanoparticle concentration of 1 wt %. It was also observed that the concentration and the dispersion homogeneity of nanoparticles favorably affected the specific heat enhancement of the molten salt nanofluids. The dispersion status of graphite nanoparticles into the salt mixtures was visualized via scanning electron microscopy. The experimental results were explained according to the nanoparticle-induced compressed liquid layer structure of the molten salts.

Keywords: nanofluids; molten salt; specific heat; compressed liquid layer; nanoparticle dispersion; thermal energy storage

1. Introduction

Nanofluids have attracted considerable attention in heat-transfer fields because of their enhanced thermal properties, such as their thermal conductivity and boiling characteristics. In 1993, Masuda et al. measured the thermal conductivity of suspensions in which Al_2O_3 , SiO_2 , and TiO_2 were dispersed in water. Authors reported that the thermal conductivity linearly increased with the particle volume concentration [1]. In 1995, Choi and Eastman proposed nanofluids as innovative heat-transfer fluids, owing to their enhanced thermal conductivity [2]. In the early 2000s, the dramatic increase of the critical heat flux in pool boiling of nanofluids gave rise to the consideration of nanofluids as an alternative to conventional heat-transfer fluids [3,4]. After those publications, related studies into the thermal property and boiling characteristic have been actively performed under various experimental conditions. As reviewed by Wang and Mujumdar, various measurement techniques for the thermal conductivity of nanofluids, such as the hot-wire method, the steady-state parallel-plate technique, and the temperature oscillation method, have been employed [5]. Various kinds of nanoparticles have been dispersed into base fluids—generally water, oil, and ethylene glycol—to examine the enhancements in the thermal conductivity (summarized in [5,6]). The significantly enhanced critical heat flux in pool boiling of nanofluids was also evaluated to be outstanding. This has been attributed to the change of the surface wettability due to nanoparticle deposition on heater surfaces. After the observation

in these pool-boiling experiments, initially modified heater surfaces were employed to confirm the critical heat flux performance [7,8]. Significant enhancements in the critical heat flux were acquired from previous studies with the heater surface modified by nanomaterials [9–12].

While numerous studies on the thermal conductivity of nanofluids have been published, few studies on the specific heat of nanofluids have been performed, and they report that the specific heat of nanofluids decreases with the addition of nanoparticles [13–16]. Since Nelson et al. reported that the specific heat of a polyalphaolefin (PAO) nanofluid was significantly increased by adding a small amount of graphite nanoparticle fibers [17], several research groups reported that the specific heat is increased by adding nanoparticles. In particular, Dr. Banerjee's research groups reported that the specific heat of binary molten salt mixtures (or eutectic), which are considered as thermal energy storage media in concentrating solar power plants, can be enhanced via doping with nanoparticles. They used various molten salts (carbonate salts, nitrate salts, and chloride salts) as base fluids, along with both organic and inorganic nanoparticles. A wide range of parametric studies (effects of the nanoparticle concentration, particle shape, size, dispersion quality, etc.) have been performed to identify the mechanism underlying the specific heat increase in the molten salt nanofluids [18–22]. Chieruzzi et al. enhanced the specific heat of a binary nitrate ($\text{NaNO}_3\text{--KNO}_3$) by dispersing various nanoparticles (Al_2O_3 , SiO_2 , TiO_2 , and $\text{SiO}_2\text{--Al}_2\text{O}_3$) [23,24]. The enhanced specific heat of the molten salt nanofluids was explained in various ways, e.g., electron microscope images and molecular dynamics simulation [25–30]. Furthermore, a fundamental experimental study into thermal property variations of carbonate salt mixtures was performed using a differential scanning calorimeter (DSC) [31]. Additionally, the viscosity of the molten salt nanofluids was measured at a high temperature of 550 °C [32]. Most recently, Grosu et al. reported the effect of nanoparticles on the corrosivity of nitrate molten salt [33].

The publications of the diverse aforementioned studies led to extensive research for enhancing the specific heat of molten salts. Qiao et al. reported numerical and experimental results for enhancing the specific heat of a binary nitrate salt mixture [34]. In 2017, Luo et al. reported that the mixture of sodium nitrate and potassium nitrate was enhanced by CuO nanoparticles that are produced in situ via the high-temperature decomposition of copper oxalate with the nitrate salt mixture [35]. Most recently, in situ synthesized MgO nanoparticles enhanced the specific heat of a nitrate salt by up to 118% in the solid phase and 168% in the liquid phase [36]. Mondragon et al. explained the specific heat enhancement of molten salts according to the ionic exchange capacity of nanoparticles using Fourier-transform infrared spectroscopy tests [37].

Numerous studies have been performed to elucidate the specific heat increase of molten salt nanofluids and identify the mechanisms underlying the specific heat enhancement. However, the reason for the increase in the specific heat of molten salt nanofluids has not been clearly investigated. According to previous studies [20,28], the increase of the specific heat of nanofluids is not solely a result of the nanoparticles, but is closely associated with interactions between the nanoparticles and the base fluids. For effectively harnessing thermal energy storage media, such as molten salt mixtures, it is important to understand their specific heat-enhancing mechanism.

In this study, the specific heat of binary carbonate salt mixture-based graphite nanofluids was experimentally measured using a DSC. Several parameters—the chemical composition of the base fluid, the nanoparticle concentration, and the dispersion homogeneity of nanoparticles—were investigated, which are considered as influential parameters for the specific heat enhancement of nanofluids. Five different compositions of the base fluid (mole fraction of two salt components) were prepared, and the thermal property was measured for fixed nanoparticle concentrations. Conversely, the specific heat of the nanofluids was examined as the concentration of the nanoparticles varies for the uniform chemical composition of the base fluid. Moreover, concerning the dispersion of the nanoparticles, concentrations of a surfactant, used in order for the nanoparticles to be well dispersed, were also increased to appraise the effect of the particle dispersion. The experimental results obtained in this study helps us in understanding quantitative effects of each parameter on enhancing specific heat of the molten salt mixture by doping with the nanoparticles.

2. Nanofluid Synthesis and Specific Heat Measurements

2.1. Materials

Binary carbonate salt mixtures were employed as a base fluid of the nanofluids in this study. The base fluids were composed of lithium carbonate (Li_2CO_3 , Sigma-Aldrich, St. Louis, MO, USA) and potassium carbonate (K_2CO_3 , Sigma-Aldrich, St. Louis, MO, USA) in various mole fractions. According to a previous study [38], lithium carbonate and potassium carbonate have a eutectic composition (62 mol % of Li_2CO_3 and 38 mol % of K_2CO_3) in which the carbonate salt eutectic has a high melting temperature of 488 °C. Recently, Jo and Banerjee reported that the specific heat of carbonate salt mixtures in the liquid phase changes drastically with the molar fraction of the two salts [31]. As mentioned previously, the base fluid (chemical composition of two salts in a binary salt mixture) affects the enhancement of the specific heat of the salt mixtures as well [28]. For this reason, five different salt compositions were chosen for the base fluid of the nanofluid tested in this study. Graphite nanoparticles (Sigma-Aldrich, St. Louis, MO, USA) less than 50 nm in diameter were dispersed into the base carbonate salt mixtures. Figure 1 shows a transmission electron microscope (TEM, JEOL JSM-2010) image of the graphite particle. Gum arabic (GA, Sigma-Aldrich, St. Louis, MO, USA)—a dispersing agent for carbon nanoparticles, particularly carbon nanotubes in water [39,40]—was added for the homogeneous dispersion of the graphite nanoparticles. GA was observed to be appropriate for molten salt-based carbon nanoparticle nanofluids, compared with conventional surfactants such as sodium dodecyl sulfate and sodium dodecyl benzene sulfonate [21]. All the chemical agents were used as received.

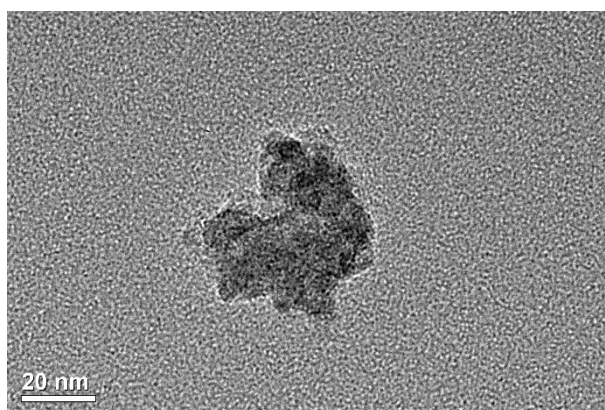


Figure 1. TEM image of a graphite nanoparticle.

2.2. Synthesis of Nanofluids

Figure 2 shows the procedures for synthesizing the molten salt-based graphite nanofluids [20,28]. First, graphite nanoparticles were dispersed into distilled water with the GA (1 wt %). Then, the aqueous graphite suspension (aqueous nanofluid) was sonicated in an ultrasonic bath (Branson 2510) for 2 h. After the sonication process, the water–salt solution was added to the graphite nanofluid. The mixture (graphite suspension and water–salt solution) was subjected to the sonication process again for 3 h. Finally, the water was removed via evaporation on a hot plate at 100 °C using a large petri dish 10 cm in diameter. After the water was completely evaporated, the dry power of the molten salt nanofluids was scraped from the entire whole petri dish, and lastly, a grinding and mixing process was performed to obtain a uniform chemical composition of the base fluid. Pure salt mixtures were prepared though the same procedures but were subjected to sonication only once, for 2 h.

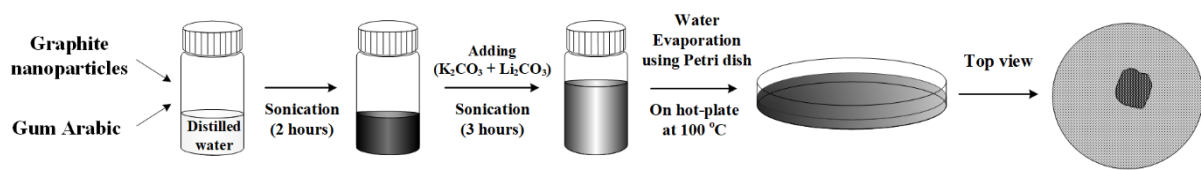


Figure 2. Synthesis procedures for molten salt nanofluids.

Two sample groups were prepared in this study: Group 1 and Group 2. With the nanofluids in Group 1, the effect of the base fluid (chemical composition of the two carbon salts) on the increase of the specific heat was investigated. That is, in the Group 1 samples, the chemical composition of the base fluid was varied, and the nanoparticle concentration was fixed. In contrast, the nanofluids of Group 2 were used to explore the effect of the nanoparticle concentration on the specific heat. Therefore, the chemical composition of the base fluid (mole fraction of the two salts) was fixed (75 mol % of Li_2CO_3 and 25 mol % of K_2CO_3), and the concentration of the graphite nanoparticles was varied from 0.025 to 1.0 wt %. As reported in a previous study [31], because the specific heat of the binary carbonate salt mixtures is strongly influenced by the chemical composition of the base salt, the mole fraction of the two salt components (lithium carbonate and potassium carbonate) was experimentally measured using inductively coupled plasma-mass spectrometry (ICP-MS) for the sample after DSC tests.

The mole fractions of the base fluid for the nanofluids in Group 1, which were measured via ICP-MS, are presented in Table 1. The mole fraction of lithium carbonate varied from 40% to 90%, and the mole fraction of potassium carbonate varied from 10% to 60%. The initial concentrations of graphite nanoparticles were 0.1 and 1.0 wt %, and GA of 1 wt % was included in each nanofluid. The mole fraction of lithium carbonate and potassium carbonate for the Group 2 nanofluids was 75:25 in molar ratio, where the maximum specific heat was measured for the binary carbonate salt mixtures in a previous study [31]. The mole fractions of the base fluid obtained via ICP-MS for the Group 2 nanofluids were not exactly the same for all of the samples. However, the deviations in the mole fraction of the two salts were between 0.8 and 1.9 mol %, which is acceptable for analyzing measurements of the specific heat. Finally, the amount of GA was increased to 5 wt % to improve the dispersion homogeneity of the nanoparticles. The specific heat of the nanofluids produced with GA of 5 wt % was compared with that of other nanofluids with GA of 1 wt % for the same base fluid and nanoparticle concentration.

Table 1. Chemical compositions and specific heat of carbonate salt mixtures for Group 1 samples.

Sample Name	Mole Fraction of Each Salt		Specific Heat in Liquid Phase [J/g·K]
	Li_2CO_3 [mol %]	K_2CO_3 [mol %]	
Sample 1	90	10	2.582
Sample 2	80	20	2.503
Sample 3	62	38	1.646
Sample 4	50	50	1.543
Sample 5	40	60	1.325

2.3. Specific Heat Measurements

The specific heat was measured using a DSC (TA Instruments, New Castle, DE, USA, Q20) up to 560 °C with a ramping rate of 20 °C/min. According to the measured heat-flow data, the specific heat of the nanofluids was determined via the standard test method ASTM E1269 [41]. For every measurement, DSC runs of an empty pan (denoted as “baseline run”) and sapphire (denoted as “sapphire run”) were conducted prior to DSC runs of the nanofluid (denoted as “sample run”) and were employed to calculate the specific heat of each nanofluid. The specific heat capacity in the liquid phase was averaged within the temperature range of 525 to 555 °C. Avoiding inaccurate measurements

of the heat flow supplied to the aluminum pans due to the warming of the heaters in the calorimeter, we executed a heating cycle with the same ramping rate in the DSC and maintained an isothermal state of 560 °C for more than 5 min prior to recording the heat flows. Hermetically sealed aluminum pans were employed for the sample runs to prevent mass loss during the thermal cycles. The same thermal cycle from 150 to 560 °C was repeated five times for the sample runs to check for variations and deteriorations in the specific heat of the nanofluids. Finally, the enhancements were calculated as follows.

$$\text{Enhancement}[\%] = \frac{c_{p,\text{Nanofluid}} - c_{p,\text{pure}}}{c_{p,\text{pure}}} \times 100 \quad (1)$$

The specific heat of pure carbonate salt eutectic was measured in this study to check the sample preparation and measurement protocol by comparing the measurement to a reference value. On the other hand, the specific heat values of the pure salt mixtures were obtained from a previous study [31] in which the specific heat was measured via the same protocol employed in this study. Using the specific heat values of the pure salt mixtures, the specific heat enhancement was determined for each nanofluid. According to our experimental measurements, it was observed in this study that the GA cannot increase the specific heat of the carbonate salt mixtures. Moreover, it is well known that the GA is thermally decomposed between 250 and 350 °C [42]. Therefore, the GA is decomposed during the first DSC ramping process. For these reasons, the effect of the GA on the specific heat increase of the molten salt nanofluids is negligible or even unfavorable. Hence, the increase of the specific heat is solely attributed to the nanoparticles dispersed into the salt mixture. Scanning electron microscopy (SEM, JSM-7500F, JEOL, Japan) was used to capture images of the nanoparticles in the salt mixtures and examine the dispersion homogeneity of the nanoparticles.

2.4. Uncertainty Analysis

As mentioned previously, the specific heat capacity was determined via the ASTM method, as follows.

$$c_s = c_{st} \frac{\Delta q_s \cdot m_{st}}{\Delta q_{st} \cdot m_s} \quad (2)$$

Here, c is the specific heat, Δq is the heat-flow difference between the specimen and the pan, m is the mass, the subscript s indicates the specimen, and the subscript st indicates the standard materials (sapphire in this study). The experimental uncertainty is represented as follows [43].

$$\frac{U_{c_s}}{c_s} = \sqrt{\left(\frac{U(c_{st})}{c_{st}}\right)^2 + \left(\frac{U(\Delta q_s)}{\Delta q_s}\right)^2 + \left(\frac{U(\Delta q_{st})}{\Delta q_{st}}\right)^2 + \left(\frac{U(m_s)}{m_s}\right)^2 + \left(\frac{U(m_{st})}{m_{st}}\right)^2} \quad (3)$$

The uncertainty resulted from the curve-fitting specific heat of sapphire, the heat flow of the specimen and the sapphire, and the mass of the specimen and the sapphire. The uncertainties of the curve-fitted specific heat of the sapphire and heat flow are $\pm 0.3\%$ and $\pm 2\%$, respectively. The maximum uncertainty in the determination of the specific heat capacity is estimated as $\pm 2.8\%$.

3. Results and Discussion

The specific heat of the pure carbonate salt eutectic (62 mol % of Li_2CO_3 and 38 mol % of K_2CO_3) was measured prior to the specific heat measurements of the nanofluids. The specific heat of the pure eutectic was 1.646 [J/g·K], which exhibits good accordance with the value of 1.6 [J/g·K] reported by Araki et al. [44]. As shown in Figure 3, the heat-flow curve of the pure eutectic exhibits typical features, such as a linearly increasing specific heat in the solid phase and an almost uniform specific heat in the liquid phase. The specific heat values of the pure salt eutectic measured in this study and the pure salt mixtures obtained from the previous study are presented in Table 1. Additionally, the specific heat of the carbonate salt eutectic–1 wt % GA mixture was measured to examine whether the GA increased the specific heat of the molten salt mixtures. The specific heat of the eutectic–GA mixture was

measured to be 1.592 [J/g·K], which is approximately 3.3% lower than that of the pure eutectic. Thus, the GA is not attributed to the specific heat increase of the molten salt nanofluids. For the nanofluids, the enhancement of the specific heat was calculated using the specific heat values of the pure salt mixtures shown in Table 1.

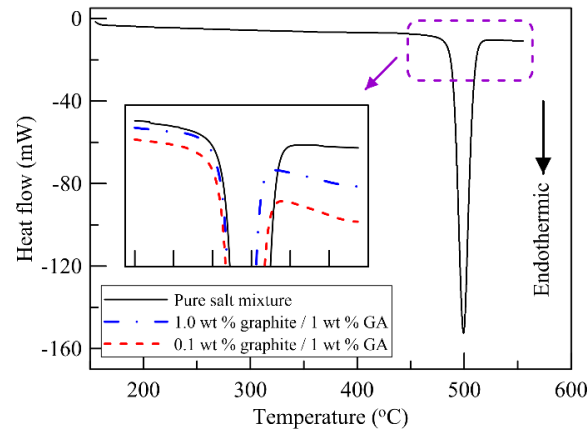


Figure 3. Heat-flow curves of the pure salt eutectic and the nanofluids, obtained via DSC measurements.

Figure 4 shows the variation of the specific heat of the nanofluids with GA of 1 wt % (Group 1) with the changing mole fraction of the two carbonate salts in the base fluid. As observed in Figure 4, the specific heat of the pure salt mixture in the liquid phase drastically increases with the increase of the lithium carbonate around the eutectic composition with the increase of lithium carbonate salt. Regarding the specific heat of the molten salt nanofluids, the increment in the specific heat was measured to be higher in the nanofluids whose composition was far from the eutectic point (62 mol % of Li_2CO_3). For instance, the increment of the specific heat for sample 5 (90 mol % of Li_2CO_3) was higher than that for sample 4 (80 mol % of Li_2CO_3) in both the 0.1 and 1.0 wt % conditions. The enhancement of the specific heat exhibited a similar increment. This feature is clearly indicated by the enhancement graph of Figure 5. The enhancements of the specific heat for the nanofluids with the chemical composition of sample 1 (90:10) were 20.0% and 25.4% for the nanoparticle concentrations of 0.1 and 1.0 wt %, respectively. For the nanofluids with the chemical composition of sample 5 (40:60), the specific heat enhancements were 21.6% and 30.1% for nanoparticle concentrations of 0.1 and 1.0 wt %, respectively. However, the specific heat enhancements for the nanofluids with the chemical compositions of samples 2 and 4 were between 12.2% and 24.8%. The enhancements for salt mixtures 2 and 4 were smaller than those for samples 1 and 5. This distinctive feature is indicated by a V-shaped bar graph with the eutectic composition as the center in Figure 5. According to these results for the specific heat of the molten salt nanofluids, two possible issues are important for understanding the increase of the specific heat of the binary carbonate salt mixtures: the concentration of nanoparticles and the dispersion homogeneity of nanoparticles.

Moreover, stability of the enhanced thermal characteristics of the nanofluids has been considered to be a significant issue. For engineering applications, the stability should be examined. In this study, the DSC thermal cycles (specific heat measurements) were repeated 5 times for the same samples to check whether or not the degradation of the specific heat enhanced was arisen. Figure 6 shows the specific heat ratio to the first cycle measurement. In other words, Figure 6 represents the relative change of the specific heat of the molten salt nanofluids to the specific heat measured at the first thermal cycle in DSC. As shown in Figure 6, no remarkable decrease was not found except one case (nanoparticle concentration of 0.1 wt % for the base fluid containing 62 mol % Li_2CO_3). Although a little decrease was observed as repeating thermal cycles (liquefaction and solidification), the degradations for most nanofluids were less than 10%. Thus, the nanofluid synthesis protocol employed in this study is appropriate for molten salt-based nanofluids. However, relatively large decreases were also observed

in a case. Hence, the stability of the nanofluids is a significant issue for engineering applications like thermal energy storage.

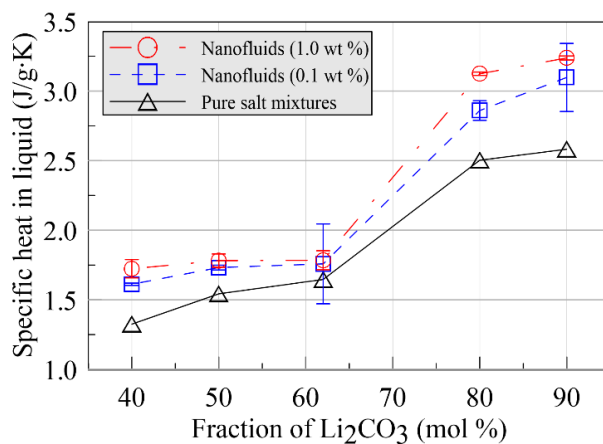


Figure 4. Specific heat of pure carbonate salt mixtures and nanofluids in the liquid phase.

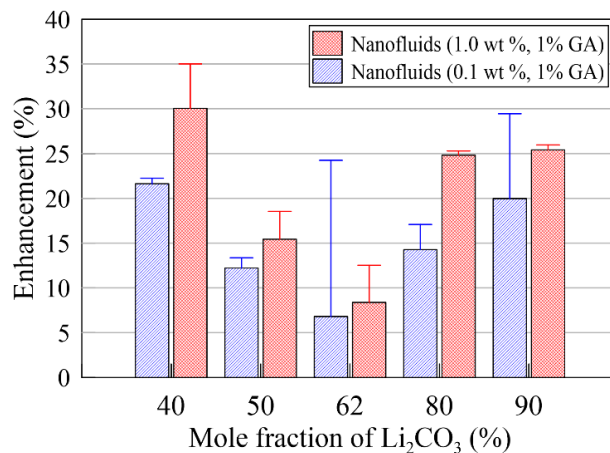


Figure 5. Enhancements of the specific heat for five different chemical compositions of base fluid.

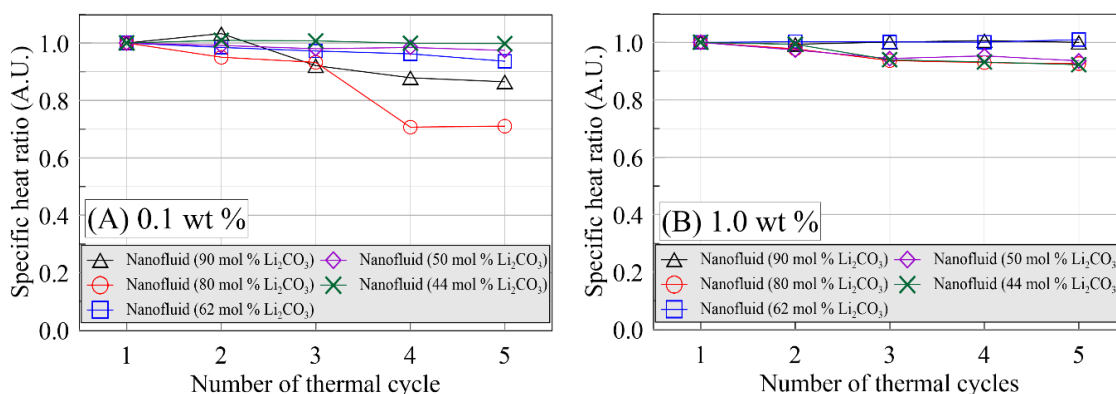


Figure 6. Change of specific heat ratio comparing to the first cycle measurement: (A) 0.1 wt % nanoparticle concentration; (B) 1.0 wt % nanoparticle concentration.

To examine the effects of the nanoparticle concentration and the dispersion, additional nanofluid samples were prepared as Group 2, and the specific heat was measured using the DSC. As mentioned in

the previous section, the chemical compositions of the base fluid were identical for all of the samples in Group 2, and the concentrations of the nanoparticles were 0.025, 0.05, 0.1, and 1.0 wt %. Figure 7 shows the specific heat of the nanofluids in both the solid phase (averaged between 390 and 410 °C) and the liquid phase. The results for the solid phase are not readily convincing, because of the large increase even in the case of doping the salt mixture with small amounts of nanoparticles. However, in a previous study, a similar result was reported for carbonate salt mixture–graphite nanofluids [28]. A nanoparticle concentration of only 0.1 wt % led to a specific heat enhancement of more than 30% for a carbonate salt mixture with almost the same chemical composition of the two salts [20]. In addition, it appeared that the increase of the specific heat was limited even though the nanoparticle concentration increased. The specific heat increase was not significant for either the solid or liquid phases. Therefore, dispersing an abundant amount of the nanoparticles is meaningless, because surplus nanoparticles result in the agglomeration of the nanoparticles; thus, the addition of nanosized-particles is no longer effective. In the liquid phase, the effect of the nanoparticle concentration on the increase of the specific heat was observed, as shown in Figure 7. The specific heat of the nanofluids was measured to exceed 3.1 [J/g·K] at a nanoparticle concentration of 1.0 wt %, which is almost double that of the pure carbonate eutectic.

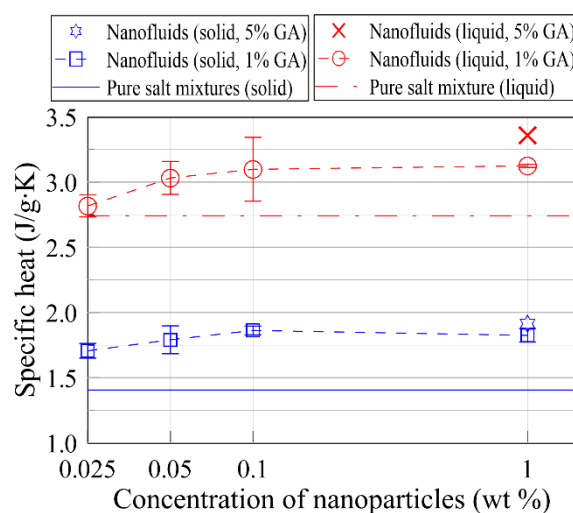


Figure 7. Specific heat of nanofluids in the solid and liquid phases with respect to the nanoparticle concentration.

The dispersion of nanoparticles has been a fundamental issue since the early stages of nanofluid research. The two-step synthesis method for the molten salt nanofluids employed in this study utilizes the high water solubility of the salt components, but the evaporation process may cause unfavorable agglomeration of nanoparticles. In particular, this is a critical problem for carbon nanoparticles such as graphite and carbon nanotubes, which need a surfactant to be dispersed into water. To determine the effect of the nanoparticle dispersion on the specific heat enhancement of the carbonate salt mixture, the amount of the surfactant—GA—was increased from 1 to 5 wt %, and the specific heat was compared with that of the nanofluid at the same nanoparticle concentration with 1 wt % GA. As shown in Figure 7, the specific heat values of the nanofluids with 5 wt % GA were 1.91 [J/g·K] in the solid phase and 3.36 [J/g·K] in the liquid phase. Figure 8 shows SEM images for nanofluids produced with 5 wt % GA: secondary electron images and backscatter images. These SEM images differ significantly from those in other studies. Small particles exhibiting a spherical shape in the secondary electron images (Figures 8-A and 8-B) were homogeneously dispersed into the salt mixture (base fluid) without any agglomeration. The backscatter images (Figures 8-C and 8-D) show the dispersion homogeneity of the nanoparticles, which were black-colored. The diameters of the particles in Figure 8 appear larger than those of the graphite nanoparticles shown in Figure 1. It is thus hypothesized that the particles

in Figure 8 are single structures of the nanoparticle-induced compressed liquid layer. Unfortunately, because energy-dispersive X-ray spectroscopy analysis was not performed for the images in Figure 8, our hypothesis is not verified. However, it was visually conformed that the homogeneously dispersed particles existed in the nanofluids. Even though the images in Figure 8 were obtained in solid phase, the dispersion homogeneity of the graphite nanoparticles in liquid phase was well maintained under repeating thermal cycles in DSC. According to the DSC measurements and the SEM images, it may be concluded that the homogeneous dispersion of the nanoparticles favorably influences the specific heat enhancement of the nanofluids.

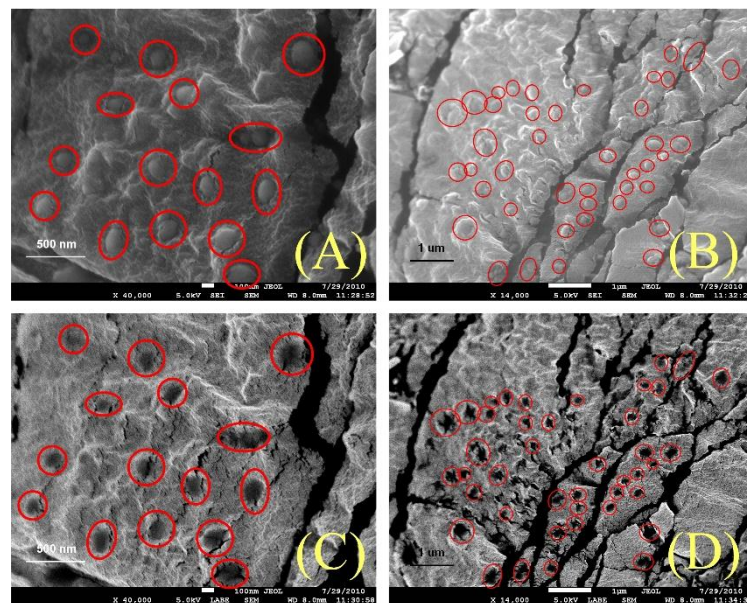


Figure 8. SEM images of the nanofluid (1 wt % nanoparticles and 5 wt % GA): secondary electron images (A,B) and backscatter images (C,D). The red circles indicate the single compressed liquid layer.

Regarding the enhanced specific heat of molten salt nanofluids, the higher heat capacity of the nanoparticles, the interfacial thermal resistance at the solid–liquid interface, and the formation of the compressed liquid layer near the nanoparticles were proposed as mechanisms contributing to the increase of the specific heat [19,23,45].

Many researchers have presented SEM images of unique structures in nanofluids. Needle-shaped structures and network-like structures are often shown in research papers concerning the specific heat of molten salt nanofluids [23,45]. It is reasonable to consider that the special structures are relevant to the specific heat increase. Oh et al. experimentally observed ordered liquid aluminum atoms adjacent to the crystalline interface with sapphire [46]. Additionally, molecular dynamics simulations showed the formation of a dense (compressed) layer with a certain thickness at the interface between a solid nanoparticle and liquid molecules [30]. This compressed liquid layer in which the solvent molecules (molten salt molecules) acquire an ordered structure can be regarded as a quasi-crystalline structure. The compressed liquid layer of binary carbonate salt mixtures has different chemical compositions of the two salts from the overall (bulk) compositions of the base fluid [20,28]. The compressed liquid layer has a higher concentration of potassium carbonate than the bulk salt mixture (base fluid). Because of the different chemical composition of the compressed liquid layer, this region has significantly different thermophysical properties than the bulk salt mixture (base fluid) [31]. Thus, the compressed liquid layers adjacent to the nanoparticles create special structures by joining each layer, and these structures enhance the specific heat of the nanofluids. Ultimately, the compressed liquid layers amplify the capacity of the nanofluids for thermal energy storage.

Figure 9 shows the nanoparticle-induced compressed liquid layer structures of the molten salt mixtures in solid phase. The network like structures in Figure 9 are presumed as the compressed liquid layer structures in solid phase. The dispersion effect can be explained by these special structures of the solvent material. If the nanoparticles are homogeneously dispersed in the base fluid, a significantly larger volume of the compressed liquid layers can be formed, and the compressed liquid layer structures should be increased. Thus, the individually dispersed nanoparticles shown in Figure 8 allow a large volume of the compressed liquid layer structures to be created in the nanofluids. Regarding the concentration effect of the nanoparticles, the specific heat of the nanofluids can be modified significantly via doping with a minute concentration of the nanoparticles in the salt mixtures, and the enhancement increases with the nanoparticle concentration. However, experimental analysis, such as energy dispersive spectroscopy, is necessary to reveal the identity of the structures in Figure 9.

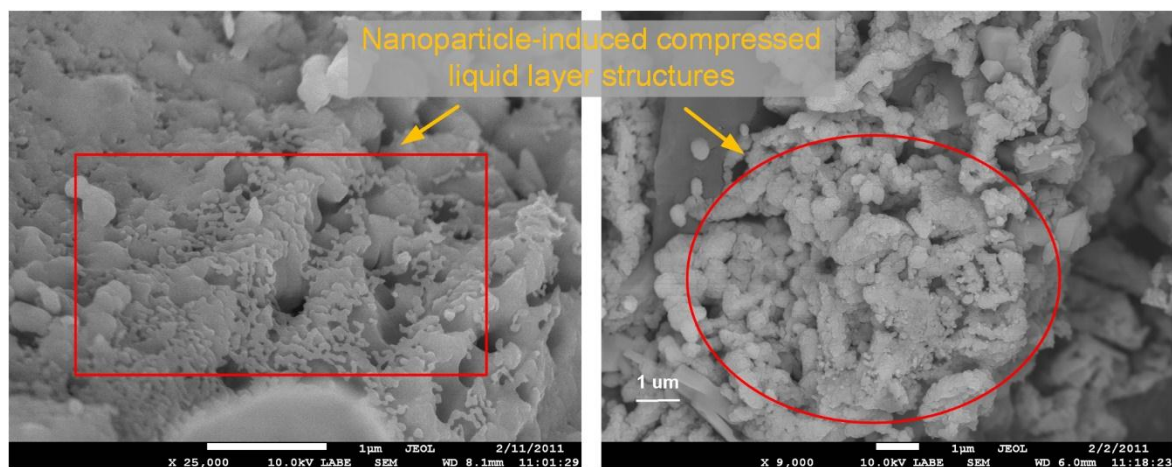


Figure 9. SEM images of the nanofluid (1 wt % nanoparticle and 5 wt % GA): nanoparticle-induced compressed liquid layer structures in solid phase.

Conventional theoretical models are unable to explain and predict the specific heat enhancements achieved in this study. While the thermal equilibrium model suggested by Buongiorno [47] is known to predict well the specific heat of aqueous nanofluids, it is only applicable for conventional nanofluids—not molten salt nanofluids—because it fails to predict the increase of the specific heat. Thus, in addition to experimental works, intensive theoretical studies on the specific heat of nanofluids—particularly high-temperature nanofluids—are needed to determine the parameters and elucidate the physics resulting in the enhanced specific heat.

4. Conclusions

The specific heat of the carbonate salt mixture-based graphite nanofluids was measured within a wide temperature range of 150–560 °C. The effects of the chemical compositions of the base fluid, the nanoparticle concentration, and the dispersion homogeneity on the specific heat were investigated. The knowledge gained in this study is summarized as follows.

- The specific heat was anomalously enhanced by up to >30% in the liquid phase and 36% in the solid phase via the dispersion of graphite nanoparticles. The enhancements were strongly dependent on the chemical composition of the base fluid: the increments, as well as the enhancements in the specific heat, increased when the chemical composition of the base fluid was far from the eutectic composition.
- The specific heat increased with the concentration of the nanoparticles. A noticeable increase was observed at the nanoparticle concentration of 0.025 wt % for the base fluid including 75 mol %

- lithium carbonate and 25 mol % potassium carbonate. A critical concentration of nanoparticles was observed. For nanoparticle concentrations exceeding 0.1 wt %, the increment was negligible.
- (c) The specific heat enhancements increased as the amount of the surfactant (GA) increased from 1 to 5 wt %. Larger enhancements were measured for the nanofluids with 5 wt % GA, and the actual specific heat value was almost double that of the eutectic.
 - (d) The homogeneous dispersion of the graphite nanoparticles was visually confirmed via SEM (secondary electron images and backscatter images) for the nanofluid after a DSC test. In the SEM images, the graphite nanoparticles were spherical, having smooth curvature (not disks), so it was presumed that special structures, nanoparticle-induced compressed liquid layer, were formed in the nanofluids. The SEM images conclusively proved that the dispersion homogeneity (quality) of the nanoparticles is due to the specific heat enhancements of the nanofluids.

Author Contributions: Hyun Jung Kim analyzed the data; Byeongnam Jo performed the experiments, analyzed the data and wrote the paper. All authors have read and approved the final version of the paper.

Acknowledgments: This work was supported partly by the New Faculty Research Fund of Ajou University and partly by the Basic Science Research Program through the National Research Foundation of Korea (NRF) funded by the Ministry of Education (NRF-2018RIA2B2001082).

Conflicts of Interest: The authors declare no conflict of interest.

References

- Masuda, H.; Ebata, A.; Teramae, K. Alternation of thermal conductivity and viscosity of liquid by dispersing ultra-fine particles (Dispersion of γ - Al_2O_3 , SiO_2 , and TiO_2 ultra-fine particles). *Netsu Bussei* **1993**, *4*, 227–233. [[CrossRef](#)]
- Choi, S.U.S.; Eastman, J.A. Enhancing thermal conductivity of fluids with nanoparticles. In Proceedings of the International Mechanical Engineering Congress and Exhibition, San Francisco, CA, USA, 12–17 November 1995.
- You, S.M.; Kim, J.H.; Kim, K.H. Effect of nanoparticles on critical heat flux of water in pool boiling heat transfer. *Appl. Phys. Lett.* **2003**, *83*, 3374–3376. [[CrossRef](#)]
- Jo, B.; Jeon, P.S.; Yoo, J.; Kim, H.J. Wide range parametric study for the pool boiling of nano-fluids with a circular plate heater. *J. Vis.* **2009**, *47*, 407–411.
- Wang, X.; Mujumdar, A.S. Heat transfer characteristics of nanofluids: A Review. *Int. J. Therm. Sci.* **2007**, *46*, 1–19. [[CrossRef](#)]
- Kebllinski, P.; Eastman, J.A.; Cahill, D.G. Nanofluids for thermal transport. *Mater. Today* **2005**, *8*, 36–44. [[CrossRef](#)]
- Kim, S.J.; Bang, I.C.; Buongiorno, J. Effects of nanoparticle deposition on surface wettability influencing boiling heat transfer in nanofluids. *Appl. Phys. Lett.* **2006**, *89*, 153107. [[CrossRef](#)]
- Kim, H.D.; Kim, J.; Kim, M.H. Experimental studies on CHF characteristics of nano-fluids at pool boiling. *Int. J. Multiph. Flow* **2007**, *33*, 691–706. [[CrossRef](#)]
- Ujereh, S.; Fisher, T.; Mudawar, I. Effects of carbon nanotube arrays on nucleate pool boiling. *Int. J. Heat Mass Transf.* **2007**, *50*, 4023–4038. [[CrossRef](#)]
- Sathyamurthi, V.; Ahn, H.S.; Banerjee, D. Subcooled pool boiling experiments on horizontal heaters coated with carbon nanotubes. *J. Heat Transf.* **2009**, *131*, 071501. [[CrossRef](#)]
- Chen, R.; Lu, M.; Srinivasan, V. Nanowires for enhanced boiling heat transfer. *Nano Lett.* **2009**, *9*, 548–553. [[CrossRef](#)] [[PubMed](#)]
- Kim, S.; Kim, H.D.; Kim, H. Effects of nano-fluid and surfaces with nano structure on the increase of CHF. *Exp. Therm. Fluid Sci.* **2010**, *34*, 487–495. [[CrossRef](#)]
- Namburu, P.K.; Kulkarni, D.P.; Dandekar, A. Experimental investigation of viscosity and specific heat of silicon dioxide nanofluids. *Micro Nano Lett.* **2007**, *2*, 67–71. [[CrossRef](#)]
- Zhou, S.; Ni, R. Measurement of the specific heat capacity of water-based Al_2O_3 nanofluid. *Appl. Phys. Lett.* **2008**, *92*, 1–3. [[CrossRef](#)]

15. Vajjha, R.S.; Das, D.K. Specific heat measurement of three nanofluids and development of new correlations. *J. Heat Transf.* **2009**, *131*, 071601. [\[CrossRef\]](#)
16. Zhou, L.; Wang, B.; Peng, X. On the specific heat capacity of CuO nanofluid. *Adv. Mech. Eng.* **2010**, *2010*, 1–4. [\[CrossRef\]](#)
17. Nelson, I.C.; Banerjee, D.; Ponnappan, R. Flow loop experiments using polyalphaolefin nanofluids. *J. Thermophys. Heat Transf.* **2009**, *23*, 752–761. [\[CrossRef\]](#)
18. Shin, D.; Banerjee, D. Enhanced specific heat of silica nanofluid. *J. Heat Transf.* **2011**, *133*, 024501. [\[CrossRef\]](#)
19. Shin, D.; Banerjee, D. Enhancement of specific heat capacity of high-temperature silica-nanofluids synthesized in alkali chloride salt eutectics for solar thermal-energy storage applications. *Int. J. Heat Mass Transf.* **2011**, *54*, 1064–1070. [\[CrossRef\]](#)
20. Jo, B.; Banerjee, D. Enhanced specific heat capacity of molten salt-based nanomaterials: Effects of nanoparticle dispersion and solvent material. *Acta Mater.* **2014**, *75*, 80–91. [\[CrossRef\]](#)
21. Jo, B.; Banerjee, D. Effect of dispersion homogeneity on specific heat capacity enhancement of molten salt nanomaterials using carbon nanotubes. *J. Sol. Energy Eng.* **2015**, *137*, 011011. [\[CrossRef\]](#)
22. Jo, B.; Banerjee, D. Enhanced specific heat capacity of molten salt-based carbon nanotubes nanomaterials. *J. Heat Transf.* **2015**, *137*, 091013. [\[CrossRef\]](#)
23. Chieruzzi, M.; Cerritelli, G.F.; Miliozzi, A.; Kenny, J.M. Effect of nanoparticles on heat capacity of nanofluids based on molten salts as PCM for thermal energy storage. *Nanoscale Res. Lett.* **2013**, *8*, 448. [\[CrossRef\]](#) [\[PubMed\]](#)
24. Chieruzzi, M.; Miliozzi, A.; Crescenzi, T.; Torre, L.; Kenny, J.M. A new phase change material based on potassium nitrate with silica and alumina nanoparticles for thermal energy storage. *Nanoscale Res. Lett.* **2015**, *10*, 273–282. [\[CrossRef\]](#) [\[PubMed\]](#)
25. Tiznobaik, H.; Shin, D. Enhanced specific heat capacity of high-temperature molten salt-based nanofluids. *Int. J. Heat Mass Transf.* **2013**, *57*, 542–548. [\[CrossRef\]](#)
26. Dudda, B.; Shin, D. Effect of nanoparticle dispersion on specific heat capacity of a binary nitrate salt eutectic for concentrated solar power applications. *Int. J. Therm. Sci.* **2013**, *69*, 37–42. [\[CrossRef\]](#)
27. Ho, M.X.; Pan, C. Optimal concentration of alumina nanoparticles in molten Hitec salt to maximize its specific heat capacity. *Int. J. Heat Mass Transf.* **2014**, *70*, 174–184. [\[CrossRef\]](#)
28. Jo, B.; Banerjee, D. Effect of solvent on specific heat capacity enhancement of binary molten salt-based carbon nanotube nanomaterials for thermal energy storage. *Int. J. Therm. Sci.* **2015**, *98*, 219–227. [\[CrossRef\]](#)
29. Mohebbi, A. Prediction of specific heat and thermal conductivity of nanofluids by a combined equilibrium and non-equilibrium molecular dynamics simulation. *J. Mol. Liq.* **2012**, *175*, 51–58. [\[CrossRef\]](#)
30. Jo, B.; Banerjee, D. Molecular dynamics study on interfacial thermal resistance between organic nanoparticles and alkali molten salt mixtures. *Int. J. Multiscale Comput. Eng.* **2017**, *15*, 199–217. [\[CrossRef\]](#)
31. Jo, B.; Banerjee, D. Thermal properties measurements of binary carbonate salt mixtures for concentrating solar power plants. *J. Renew. Sustain. Energy* **2015**, *7*, 033121. [\[CrossRef\]](#)
32. Jo, B.; Banerjee, D. Viscosity measurements of multi-walled carbon nanotubes-based high temperature nanofluids. *Mater. Lett.* **2014**, *122*, 212–215. [\[CrossRef\]](#)
33. Grosu, Y.; Udayashankar, N.; Bondarchuk, O.; Gonzalez, F.; Faik, A. Unexpected effect of nanoparticles doping on the corrosivity of molten nitrate salt for thermal energy storage. *Sol. Energy Mater. Sol. Cells* **2018**, *178*, 91–97. [\[CrossRef\]](#)
34. Qiao, G.; Lasfargues, M.; Alexiadis, A.; Ding, Y. Simulation and experimental study of the specific heat capacity of molten salt based nanofluids. *Appl. Therm. Eng.* **2017**, *111*, 033121. [\[CrossRef\]](#)
35. Luo, Y.; Du, X.; Awad, A.; Wen, D. Thermal energy storage enhancement of a binary molten salt via in-situ produced nanoparticles. *Int. J. Heat Mass Transf.* **2017**, *104*, 658–664. [\[CrossRef\]](#)
36. Huang, Y.; Cheng, X.; Li, Y.; Yu, G.; Xu, K.; Li, G. Effect of in-situ synthesized nano-MgO on thermal properties of NaNO₃-KNO₃. *Sol. Energy* **2018**, *160*, 208–215. [\[CrossRef\]](#)
37. Mondragon, R.; Julia, J.E.; Cabedo, L.; Navarrete, N. On the relationship between the specific heat enhancement of salt-based nanofluids and the ionic exchange capacity of nanoparticles. *Sci. Rep.* **2018**, *8*, 7532. [\[CrossRef\]](#) [\[PubMed\]](#)
38. Janz, G.J.; Allen, C.B.; Bansal, N.P.; Murphpy, R.M.; Tomkins, R.P.T. Physical properties data compilations relevant to energy storage-2. In *Molten Salts: Data on Single and Multi-Component Salt Systems*; US Govt. Print. Off.: Washington, DC, USA, 1979; Volume 61, pp. 1–452.

39. Hilding, J.; Grulke, E.A.; Zhang, Z.G. Dispersion of carbon nanotubes in liquids. *J. Dispers. Sci. Technol.* **2003**, *24*, 1–41. [[CrossRef](#)]
40. Ding, Y.; Alias, H.; Wen, D. Heat transfer of aqueous suspensions of carbon nanotubes (CNT nanofluids). *Int. J. Heat Mass Transf.* **2006**, *49*, 240–250. [[CrossRef](#)]
41. ASTM E1269-95. *Standard Test Method for Determining Specific Heat Capacity by Differential Scanning Calorimetry*; American Society for Testing and Materials: West Conshohocken, PA, USA, 2005.
42. Daoub, R.M.A.; Elmubarak, A.H.; Misran, M.; Hassan, E.A.; Osman, M.E. Characterization and functional properties of some natural Acacia gums. *J. Saudi Soc. Agric. Sci.* **2018**, *17*, 241–249. [[CrossRef](#)]
43. Kline, S.J.; McClintock, F.A. Describing uncertainties in single-sample experiments. *Mech. Eng.* **1953**, *75*, 3–8.
44. Araki, N.; Futamura, M.; Makino, A. Measurements of thermophysical properties of sodium acetate hydrate. *Int. J. Thermophys.* **1995**, *16*, 1455–1466. [[CrossRef](#)]
45. Shin, D.; Banerjee, D. Specific heat of nanofluids synthesized by dispersing alumina nanoparticles in alkali salt eutectic. *Int. J. Heat Mass Transf.* **2014**, *74*, 210–214. [[CrossRef](#)]
46. Oh, S.H.; Kauffmann, Y.; Scheu, C.; Kapan, W.D.; Ruhle, M. Ordered liquid aluminum at the interface with sapphire. *Science* **2005**, *310*, 661–663. [[CrossRef](#)] [[PubMed](#)]
47. Buongiorno, J. Convective transport in nanofluids. *J. Heat Transf.* **2006**, *128*, 240–250. [[CrossRef](#)]



© 2018 by the authors. Licensee MDPI, Basel, Switzerland. This article is an open access article distributed under the terms and conditions of the Creative Commons Attribution (CC BY) license (<http://creativecommons.org/licenses/by/4.0/>).